J|A|C|S COMMUNICATIONS

Published on Web 06/28/2010

SnSe Nanocrystals: Synthesis, Structure, Optical Properties, and Surface Chemistry

William J. Baumgardner,*,† Joshua J. Choi,‡ Yee-Fun Lim,‡ and Tobias Hanrath*,§

Department of Chemistry and Chemical Biology, School of Applied and Engineering Physics, and School of Chemical and Biomolecular Engineering, Cornell University, Ithaca, New York 14853

Received February 16, 2010; E-mail: wjb87@cornell.edu; th358@cornell.edu

Abstract: The colloidal synthesis of SnSe nanoparticles is accomplished through the injection of bis[bis(trimethylsilyl)amino]tin(II) into hot trioctylphosphine:selenium in the presence of oleylamine. Through the manipulation of reaction temperature particles are grown with the average diameter reliably tuned to 4−10 nm. Quantum confinement is examined by establishing a relationship between particle size and band gap while the in depth growth dynamics are illuminated through UV−vis−NIR spectroscopy. Surface chemistry effects are explored, including the demonstration of useful ligand exchanges and the development of routes toward anisotropic particle growth. Finally, transient current−voltage properties of SnSe nanocrystal films in the dark and light are examined.

Colloidal IV−VI compound semiconductor nanocrystals (NCs) have garnered immense interest from fundamental and applied research communities alike. NC size, shape, and surface states have an important influence on confinement of electron and hole wave functions within the NC.[1−5] On the other hand, the influence of crystal symmetry is less understood. Lead chalcogenide NCs (PbX; X = S, Se, Te) have been a successful model system for the fundamental study of quantum confinement since their narrow energy gap and electronic structure provide access to one of the most strongly quantum confined systems, which have recently been exploited in prototype optoelectronic devices.[6−9]

To investigate the relationship between quantum confinement and NC symmetry however, alternative systems are required. The entire lead chalcogenide family exhibits cubic NaCl symmetry (space group: $Fm\bar{3}m$); by contrast tin chalcogenides exhibit a richer diversity of crystal symmetries.[10] For example, SnTe exhibits cubic NaCl symmetry, while SnO forms a tetragonal lattice (space group: $P4/nmm$) with a van der Waals gap separating the (100) planes.[11] SnSe adopts features of each, crystallizing into an orthorhombic structure (space group: *Pnma*) which may be viewed as a highly distorted NaCl lattice.[12] Alongside spatial confinement, these structural aspects, in particular the lack of dangling bonds and the stereochemical activity of the Se (5s) lone pair in SnSe, are expected to strongly influence the electronic nature of the (100) surface and the NC as a whole.[13,14] This unique combination of crystallographic and optical properties, including slow carrier relaxation rates and a mid-IR band gap (0.9 eV indirect and 1.3 eV direct), render SnSe NCs as a promising, lead-free building block for a variety of optoelectronic applications.[15]

Despite this promise, progress toward developing the potential of SnSe NCs has been slow. Recently, a synthesis of elongated, anisotropic nanocrystals of fairly large size (19 nm wide, 50−100 nm long) was reported, yet robust control over size, shape, and surface chemistry remains a significant hurdle.[16] To address this challenge, we studied the hot-injection colloidal synthesis of SnSe NCs. Beyond illustrating the relationship between NC size and the quantum confined energy gap, we discovered that SnSe NCs exhibit orthorhombic symmetry with a mixture of *Pnma* and *Cmcm* space groups, which has previously only been observed in bulk phases at high temperatures.[17,18] We analyzed fundamental NC nucleation and growth aspects and found that the SnSe NC shape is sensitive to the type of surface ligand employed during the synthesis.

While we were able to synthesize crude SnSe QDs with other tin precursors (such as tin oleate), we found the most success utilizing bis[bis(trimethylsilyl)amino]tin(II), the same precursor employed in previous reports of SnTe and SnS NC syntheses.[19,20] The synthetic method for SnSe NCs was as follows: 2 mL of 0.1 M trioctylphospine:selenium were injected into 14 mL of degassed oleylamine under an inert atmosphere. 780 μL of bis[bis(trimethylsilyl)amino]tin(II) were diluted in 6 mL of oleylamine and injected into the reaction mixture at the adjusted temperature in the range of 65 to 175 °C. Shortly after nucleation, 3 mL of oleic acid were injected into the mixture, which was quenched after 2 min. The particles were cleaned and precipitated using hexane and isopropanol as a solvent and antisolvent respectively. Energy dispersive X-ray spectroscopy confirms the nearly stoichio-

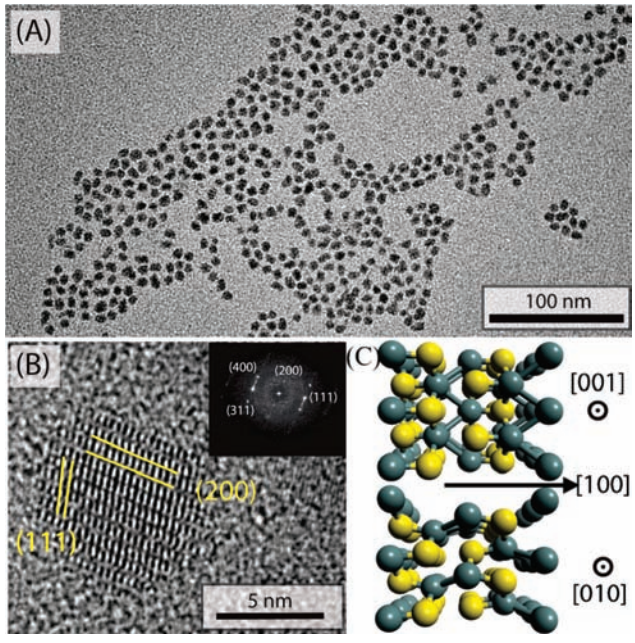

Figure 1. (a) Low resolution image of SnSe NCs synthesized at 155 °C. (b) High resolution image showing (200) and (111) lattice fringes (inset) fast Fourier transform of (b). (c) (001) and (010) projections of a model SnSe unit cell with *Pnma* symmetry.

† Department of Chemistry and Chemical Biology.
‡ School of Applied and Engineering Physics.
§ School of Chemical and Biomolecular Engineering.

metric ratio of Sn:Se (48:52). A detailed discussion of the NC synthesis is provided in the Supporting Information.

Figure 1 shows typical low- and high-resolution transmission electron micrographs (TEM) of the colloidal SnSe NCs. The TEM images illustrate two important attributes of SnSe NCs: first, the low-resolution image (Figure 1A) shows an ensemble of SnSe NCs with irregular, pseudospherical, shapes and a larger size distribution compared to the products obtained in more established colloidal PbSe NC syntheses; second, the high-resolution image in Figure 1B depicts an isolated SnSe NC with resolved (200) planes with stacking faults. Whereas crystallographic defects are rare in colloidal lead salt NCs, we commonly found these defects in SnSe NCs (see additional HRTEM images in the Supporting Information Figure S2). Both observations are consistent with the highly anisotropic crystal structure and weak bonding of the (100) planes illustrated in the crystallographic model in Figure 1C.

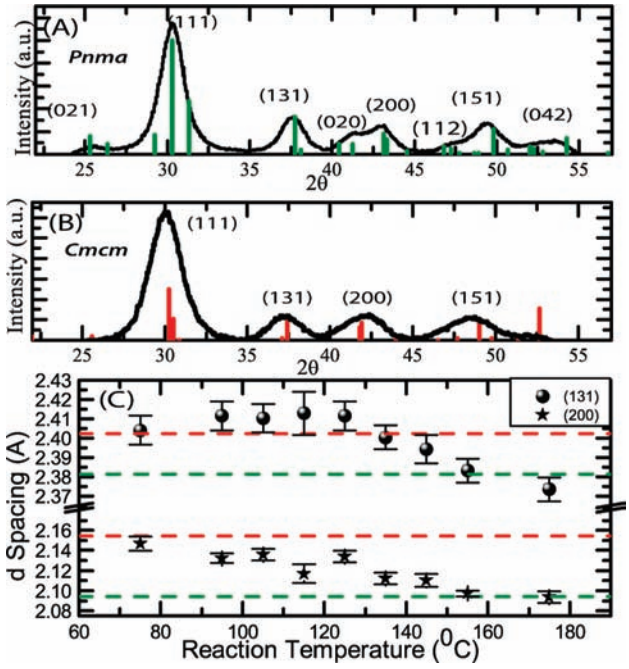

Figure 2. X-ray diffractograms of two different NC syntheses. The synthesis parameters were identical except for the injection/growth temperature. (a) Synthesized at 175 °C, presenting primarily *Pnma* crystal structure. (b) Synthesized at 105 °C and presenting primarily *Cmcm* crystal structure. (c) *d* spacing of the (131) and (200) reflections of samples synthesized at various temperatures. The colored lines represent the literature value for the *Cmcm* (red) and *Pnma (*green) space groups.

We turned to wide-angle X-ray diffraction (XRD) to gain more detailed insights into the crystallographic aspects of SnSe NCs and their relationship to synthesis conditions. Figure 2A shows the XRD pattern of NCs synthesized at 175 °C, which can be indexed to the *Pnma* crystal structure (JPCD# 32-1382). The crystal structure is further confirmed from HR-TEM and selected area diffraction (Figure S2). We applied Scherrer peak width analysis and determined the average grain size to be typically 30−40% smaller than the particle diameter determined from statistical TEM image analysis, providing further indication of high crystal defect density.

NCs synthesized at lower temperatures had a smaller average diameter but also exhibited an unexpected trend in crystal symmetry. The scattering data in Figure 2B show that SnSe NCs synthesized at 105 °C present XRD signatures with a noticeably larger *d* spacing for several reflections, providing evidence for character of *Cmcm* symmetry (JPCD #03-065-3876). In bulk SnSe crystals, the *Cmcm* structure has previously only been reported to occur after high temperature annealing (600 °C), while, in these NCs, its signature appears more pervasively at lower temperatures.[17,18] Unfortunately, the peak broadening inherent to nanoparticles, combined with the close similarity of the two crystal structures, does not allow for conclusive unambiguous assignment of one crystal structure or the other. However, systematic analysis of SnSe NCs synthesized at various temperatures revealed a clear temperature-dependent trend in the spacing of the (131) and (200) planes (Figure 2C) and a disappearance of the *Pnma*-characteristic (020) and (112) reflections.

To probe the size-dependent optical properties of SnSe NCs, we measured absorbance spectra of colloidal SnSe NC suspensions. We tuned the size of the NCs from 4 to 10 nm, which also adjusts the crystal structure, by manipulating the injection and reaction temperatures (see Supporting Information Figure S1). We then correlated the first band gap of the material to particle size using standard methods, as illustrated in Figure 3. We were further able to examine the direct band gap through a combination of absorbance and photoluminescence measurements (Supporting Information Figure S3). The quantum dots were weakly emitting, as expected from a primarily indirect band gap material. The excited state lifetime showed faster decay than 5 ns instrumental resolution. We observe confinement effects tapering off near 10 nm in both the indirect and direct band gaps. The size dependent trend in energy gap suggests that confinement effects in SnSe NCs are less pronounced than in analogous PbSe NCs, as would be expected from the strongly reduced dielectic constant (42−62 vs 210 at 300 K);[21] nevertheless, the tunable energy gaps from 0.9 to ∼1.3 eV cover the ideal range for single junction solar energy conversion.

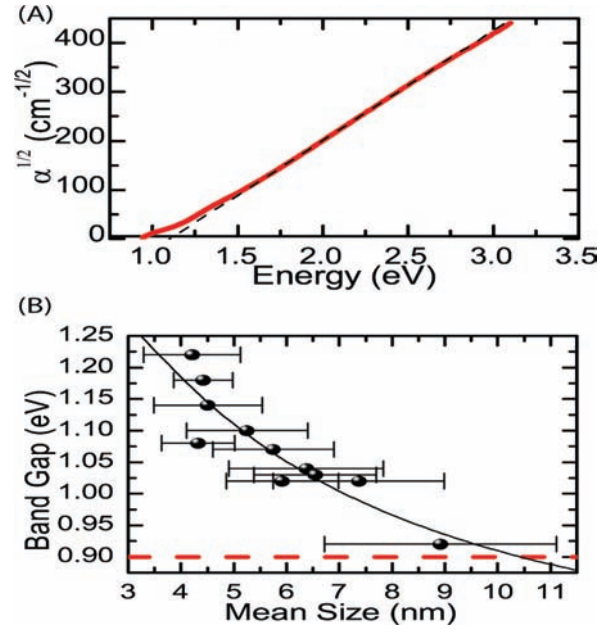

Figure 3. (a) Plot used to determine the indirect band gap of a sample of particles, developed from UV−vis−NIR data. (b) Relationship between particle size and band gap. The size of the particles was determined from TEM images. The error bars describe the distribution of particle sizes within the sample, not the uncertainty in the mean.

The relationship between NC size and optical properties provides a powerful spectroscopic signature to analyze the NC nucleation and growth dynamics in greater detail. Using ultraviolet near-infrared spectroscopy (UV−vis−NIR), we monitored the growth trajectories of NCs. We discovered that oleic acid plays drastically different roles in SnSe than in PbX colloidal NC synthesis. In the case of lead salt

NCs, oleic acid is used to tune the nucleation environment to control the number of nuclei and, ultimately, particle size.[9,22] In the colloidal synthesis of SnSe NCs, NC nucleation was inhibited if oleic acid was present prior to the injection of the tin precursor. We attribute this to the strong binding in tin oleate which lowers the chemical potential driving force for nucleation. To allow the formation of SnSe nuclei, we changed the precursor injection sequence by injecting oleic acid at specific times after mixing the Se and Sn precursors. Using optical signatures as a metric for NC size and concentration, we found that injection of oleic acid ligand accelerated the NC growth to reach an equilibrium size. Interestingly, a systematic study of different injection times showed that the final NC size distribution was independent of the time at which oleic acid was injected (see Supporting Information Figure S4).

To gain a better understanding of the organic species bound to the SnSe NC surface, we measured Fourier-transform infrared spectra (FTIR) of SnSe NC films. As-synthesized NCs showed FTIR spectral signatures consistent with that of oleic acid passivated NCs (Figure S5). Since ligand versatility is a critical aspect for many NC applications, we explored ligand exchange reactions to replace the long chain oleic acid with shorter chain thiols, dithiols, and carboxylic acids.[23,24] We displaced surface bound oleate ligands with dodecanethiol, which formed a stable NC suspension. Building on these insights, we modified the SnSe NC synthesis to replace oleic acid ligands with long chain thiols. Results show that careful tuning with dodecanethiol promotes the growth of anisotropic SnSe NCs, leading to complex elongated structures including branched superstructures (see Supporting Information Figure S6). Dithiol ligands can be used to cross-link proximate SnSe NCs. We found that ethanedithiol (EDT) readily replaces surface bound oleate ligands. EDT treated SnSe NCs are insoluble in organic and aqueous solvents. Short chain carboxylic acids, such as formic, acetic, or oxalic acid, have been shown to similarly immobilize particles, while improving electronic coupling.[25]

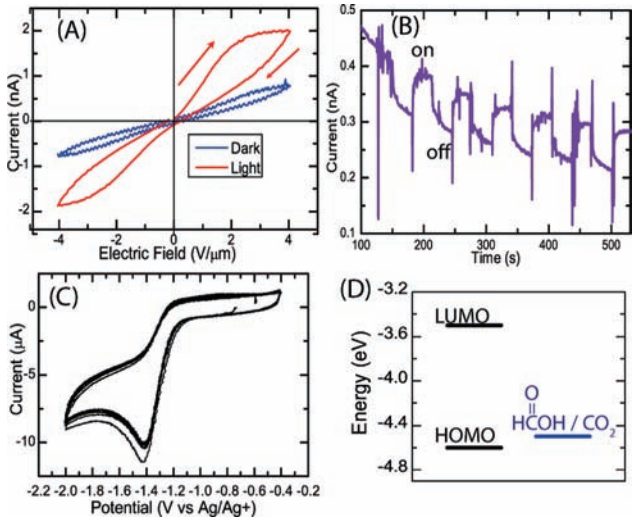

Figure 4. Current−voltage characteristics of formic acid treated SnSe NC films (a) IV curve, (b) transient photocurrent observed at a bias of 2 V/μm under 100 mW/cm^2 illumination turned on and off at 45 s intervals. (c) Cyclic voltammogram of oleic acid capped SnSe NCs using a Ag/Ag+ reference electrode and (d) corresponding HOMO−LUMO energy levels.

To test potential photovoltaic applications of SnSe NCs we measured the photocurrent of formic acid passivated SnSe NC films covering interdigitated gold electrodes. Transient current−voltage (IV) characteristics in the light and dark confirmed the photoconductivity of the particles, while revealing significant hysteresis and signal degradation (Figure 4b). Similar effects were observed in oleic acid passivated SnSe NC films (cf. Figure S7). IV hysteresis can result from charge trapping in surface states or from photoelectrochemical interactions between the NC and surface bound ligands.[26] To test the latter, we measured the SnSe NC energy levels relative to the oxidation potential of formic acid ligands using cyclic voltammetry. The energy level offsets (Figure 4d) suggest that photo-oxidation of surface bound carboxylic acid ligands is likely a key contributor to the transient photocurrent degradation. These experiments demonstrate as a proof of principle the utility of these materials for photovoltaic applications, while emphasizing the need for greater understanding of the surface chemistry to fully unlock their potential. Further device studies focusing on the integration of SnSe NCs into prototype solar cells are currently under way.

To summarize, the colloidal synthesis of SnSe QDs with size control is shown, with insights given to their crystallographic, optical, and transport properties. Further studies are under way to optimize the nanocrystals for photovoltaic and other device applications.

Acknowledgment. We thank the KAUST-CU Center for Energy and Sustainability for support. TEM and XRD characterization was performed at the Cornell Center for Materials Science. We thank the Dichtel research group at Cornell for use of their spectrophotometer. We thank Prof. Hector Abruña and Stephen Burkhardt for helpful discussions and assistance with cyclic voltammetry measurements.

Supporting Information Available: Detailed protocols, additional HRTEM images, nucleation and growth and surface chemistry experiments are included. This material is available free of charge via the Internet at http://pubs.acs.org.

References

(1) Wise, F. W. *Acc. Chem. Res.* **2000**, *33*, 773.
(2) Efros, A.; Rosen, M. *Annu. Rev. Mater. Sci.* **2000**, *30*, 475.
(3) An, J. M.; Franceschetti, A.; Dudiy, S. V.; Zunger, A. *Nano Lett.* **2006**, *6*, 2728.
(4) Wehrenberg, B. L.; Wang, C. J.; Guyot-Sionnest, P. *J. Phys. Chem. B* **2002**, *106*, 10634.
(5) Koleilat, G. I.; Levina, L.; Shukla, H.; Myrskog, S. H.; Hinds, S.; Pattantyus-Abraham, A. G.; Sargent, E. H. *ACS Nano* **2008**, *2*, 833.
(6) Sukhovatkin, V.; Hinds, S.; Brzozowski, L.; Sargent, E. H. *Science* **2009**, *324*, 1542.
(7) Choi, J. J.; Lim, Y.-F.; Santiago-Berrios, M. E. B.; Oh, M.; Hyun, B.-R.; Sun, L.; Bartnik, A. C.; Goedhart, A.; Malliaras, G. G.; Abruña, H. D.; Wise, F. W.; Hanrath, T. *Nano Lett.* **2009**, *9*, 3749.
(8) Ellingson, R. J.; Beard, M. C.; Johnson, J. C.; Yu, P.; Micic, O. I.; Nozik, A. J.; Shabaev, A.; Efros, A. L. *Nano Lett.* **2005**, *5*, 865.
(9) Urban, J.; Talapin, D.; Shevchenko, E.; Murray, C. *J. Am. Chem. Soc.* **2006**, *128*, 3248.
(10) Littlewood, P. B. *J. Phys. C: Solid State Phys.* **1980**, *13*, 4855.
(11) Pannetier, J.; Denes, G. *Acta Crystallogr., Sect. B* **1980**, *36*, 2763.
(12) Pearson, W. B. *Handbook of Lattice Spacing and Structure of Metals and Alloys*; Pergamon: London, 1976; Vol. 3.
(13) Lefebvre, I.; Szymanski, M.; Olivier-Fourcade, J.; Jumas, J. *Phys. Rev. B* **1998**, *58*, 1896.
(14) Walsh, A.; Watson, G. W. *J. Phys. Chem. B* **2005**, *109*, 18868.
(15) Pejova, B.; Tanusevski, A. *J. Phys. Chem. C* **2008**, *112*, 3525.
(16) Franzman, M. A.; Schlenker, C. W.; Thompson, M. E.; Brutchey, L. R. *J. Am. Chem. Soc.* **2010**, *132*, 4060.
(17) Bernardes-Silva, A. C.; Mesquita, A. F.; Neto, E. M.; Porto, A. O.; Ardisson, J. D.; Lima, G. M.; Lameiras, F. S. *Mater. Res. Bull.* **2005**, *40*, 1497.
(18) Chattopadhyay, T.; Pannetier, J.; Von Schnering, H. G. *J. Phys. Chem. Solids* **1986**, *47*, 879.
(19) Hickey, S. G.; Waurisch, C.; Rellinghaus, B.; Eychmüller, A. *J. Am. Chem. Soc.* **2008**, *130*, 14978.
(20) Kovalenko, M. V.; Heiss, W.; Shevchenko, E. V.; Lee, J.-S.; Schwinghammer, H.; Alivisatos, A. P.; Talapin, D. V. *J. Am. Chem. Soc.* **2007**, *129*, 11354.
(21) Madelung, O.; *Semiconductors: Non-Tetrahedrally Bounded Elements and Binary Compounds I*; Springer-Verlag: New York, 1998; p 144.
(22) Lifshitz, E.; Bashouti, M.; Kloper, V.; Kigel, A.; Eisen, M. S.; Berger, S. *Nano Lett.* **2003**, *3*, 857.
(23) Moody, I. S.; Stonas, A. R.; Lonergan, M. C. *J. Phys. Chem. C* **2008**, *112*, 19383.
(24) Seo, J.; Kim, S. J.; Kim, W. J.; Singh, R.; Samoc, M.; Cartwright, A. N.; Prasad, P. N. *Nanotechnology* **2009**, *20*, 95202.
(25) Zarghami, M. H.; Liu, Y.; Gibbs, M.; Gebremichael, E.; Webster, C.; Law, M. *ACS Nano* **2010**, *4*, 2475.
(26) Kakuta, S.; Abe, T. *ACS Appl. Mater. Interfaces* **2009**, *1*, 2707.

JA1013745